P. Suárez-Casal, Ó. Fresnedo, L. Castedo and J. García-Frías, "Analog Transmission of Correlated Sources Over Fading SIMO Multiple Access Channels," in *IEEE Transactions on Communications*, vol. 65, no. 7, pp. 2999-3011, July 2017, doi: 10.1109/TCOMM.2017.2695197.

Link to published version: https://doi.org/10.1109/TCOMM.2017.2695197

Analog Transmission of Correlated Sources over fading SIMO Multiple Access Channels

Pedro Suárez-Casal, Óscar Fresnedo *Member, IEEE*, Luis Castedo, *Senior Member, IEEE*, Javier García-Frías, *Senior Member, IEEE*

***Abstract*—Joint Source-Channel Coding for discrete-time analog sources is an appealing transmission approach because of its extremely low delay and complexity. When the users access the channel orthogonally, analog transmission of correlated information over fading Multiple Access Channels (MACs) using modulo-like mappings provides better performance than uncoded transmission. In this work, we propose a simplified decoder for modulo mappings in possibly non-orthogonal MAC scenarios with single-antenna users and a multiple-antenna receiver. Sphere decoding is investigated to reduce the computational complexity when the number of users is large. In addition, affordable strategies are proposed to optimize the mapping parameters according to the channel conditions and the source correlation. The obtained results show that the use of modulo mappings is suitable when the number of antennas at the receiver is larger than the number of users and for high correlation between user data.**

***Index Terms*—Multiuser channels, Correlation, MAP estimation, Mean square error methods**

I. Introduction

THE transmission of correlated information over fading Multiple Access Channels (MACs) is an important problem in wireless communications. Traditional approaches are based on the separate optimization of the source and the channel encoders [1]. Separation, however, presents significant practical limitations. On the one hand, optimal performance is approached as long as the block length of the encoders is large enough, and this leads to high complexity and large delays. Moreover, encoders are specifically optimized for given channel conditions. When these conditions change, the rates of the source and channel encoders must be adapted, and the separation schemes need to be completely redesigned. In addition, separation is no longer optimal for the transmission of correlated data over MACs [2], [3].

An alternative strategy is the use of Joint Source-Channel Coding (JSCC) where source and channel encoding is performed in a single operation. Different works [4], [5], [6] have already considered the use of JSCC for correlated sources over MACs, but all of them employ digital formats to transmit the user data. In this work, however, we focus on analog JSCC techniques to be applied when the source information is analog. Analog JSCC basically employs mappings based on geometric curves to transform the discrete-time continuous-amplitude source symbols into the corresponding encoded symbols [7], [8]. These mappings are based on parametric curves that fill up the source space. This strategy has been shown to closely approach the optimal performance in the case of compression of independent sources over Additive White Gaussian Noise (AWGN) channels [9], [10], [11]. It has also been applied to fading channels [12], Multiple-Input and Multiple-Output (MIMO) channels [13], bandwidth expansion [14] or the compression of correlated sources in AWGN channels [15].

We address in this work the application of analog JSCC techniques to the transmission of correlated data over fading Single-Input and Multiple-Output (SIMO) MACs with single-antenna users and a multiple-antenna receiver. We focus on non-cooperative scenarios where the users individually encode their data and the correlation is exploited at the receiver, a problem which has been studied previously for different scenarios. A particular encoder known as Scalar Quantizer Linear Coding (SQLC) was proposed to transmit bivariate Gaussian sources over Gaussian MAC [16]. It consists of a scalar quantizer and an optimized linear analog mapping. Other works also address the design of non-parametric analog mappings for the same scenario, obtaining similar shapes for the optimal mappings [17]. One of the first works focused on low delay schemes for distributed coding of bivariate correlated sources over orthogonal channels is [18], which showed that non-linear mappings are able to achieve better performance than linear approaches when the source information is correlated. Other works studied the optimal non-parametric mappings for this setup with different strategies and, interestingly, they found that such mappings resemble modulo functions [19], [20].

Analog mappings for two users orthogonal MAC with collaborative and distributed coding have also been studied [21]. In the case of distributed coding, they consider modulo functions and the mapping parameters are computed solving numerically an optimization problem. The use of modulo mappings for a general number of sources in a sensor network have been explored in [22]. In this case, the proposed mapping consists of a combination of linear and modulo mappings depending on the channel conditions. In addition, a low complexity ML decoder is proposed to estimate the common message for all sensor nodes. A more general approach is presented in [23] where analog mappings based on different lattices are considered for the transmission of multivariate Gaussian sources over orthogonal fading channels. In this

Pedro Suárez-Casal, Óscar Fresnedo and Luis Castedo are with the Department of Electronics and Systems, University of A Coruña, 15071, A Coruña, Spain, e-mail: {pedro.scasal, oscar.fresnedo, luis}@udc.es.

Javier García-Frías is with Department of Electronics, University of Delaware, USA, e-mail: jgf@delaware.edu

work, the mapping parameters are optimized numerically by searching the parameter space and a ML approach similar to [22] is also applied to estimate all the source symbols. Finally, an approximation to Maximum A Posteriori (MAP) decoding for the MAC with modulo mappings and orthogonal signaling has been considered in [24] but the proposed solution scales exponentially with the number of users.

A. Contributions

The main contributions of this work are summarized as:

- The development of a decoding algorithm based on the MAP criterion that jointly exploits the source correlation to determine estimates of the user symbols. This decoder can be applied to scenarios using MIMO or Filter Bank Multi-Carrier (FBMC) techniques, where the transmission is not necessarily orthogonal. This represents a significant difference with respect to previous works on modulo mappings [21], [22], [23]. Sphere decoding is used to reduce the computational complexity and provide affordable solutions in scenarios with large number of users. This decoding strategy is shown to exhibit a performance similar to that of optimal Minimum Mean Squared Error (MMSE) decoding.
- The performance evaluation of parametric modulo mappings for correlated sources and fading SIMO MACs. Two low complexity approaches are also proposed to optimize the users mapping parameters depending on the source correlation and the Channel State Information (CSI) available. These approaches avoid numerical optimizations of the parameters present in previous works [21], [23].

B. Notation

In this work, scalars are represented by lower case letters, vectors by bold lower case letters, and matrices by bold capital letters. The superscripts ^{T} and ^{H} are the transpose and the Hermitian operators, respectively. $\mathbb{E}[\cdot]$ and $\mathrm{tr}(\cdot)$ correspond to the mathematical expectation and the trace of a matrix, respectively. The operator $|\cdot|$ with a scalar argument represents the absolute value, with a matrix argument represents the determinant, and with a set argument represents its cardinality. The operator $\lfloor\cdot\rceil$ and $\lfloor\cdot\rfloor$ represent the element-wise round and floor operations, while $\mathrm{mod}(\mathbf{a},\mathbf{b})$ is the element-wise modulo operation that returns for each index $\mathrm{mod}([\mathbf{a}]_i,[\mathbf{b}]_i)$. The operator $\Re(\cdot)$ takes the real part of a complex-valued argument. $\mathbf{A}\otimes\mathbf{B}$ is the Kronecker product of matrices $\mathbf{A}$ and $\mathbf{B}$, $\mathrm{diag}\,(\cdot)$ is the diagonal matrix with the arguments in its main diagonal, and $\mathrm{blockdiag}\,(\cdot)$ constructs a diagonal supermatrix in which the diagonal elements are given by the matrices in the argument, and the off-diagonal elements are zero matrices. $Q(x)=\frac{2}{\sqrt{\pi}}\int_0^x \exp(-x^2)\mathrm{d}x$ denotes the Gauss error function. Finally, $\mathbf{0}$ and $\mathbf{1}$ denote the vectors of zeros and ones of the right dimension, respectively.

II. System Model

Fig. 1 shows the block diagram of the considered MAC communication model. As observed, K single-antenna users

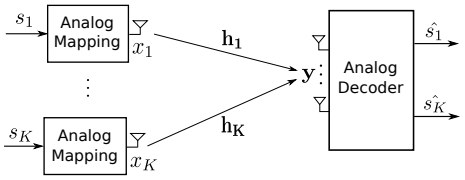

Fig. 1. Block diagram of the considered communication model.

transmit their information to a centralized receiver with N_R antennas. The multiuser source information is represented by $\mathbf{s}=[s_1,\cdots,s_K]^T\in\mathbb{C}^K$ which is assumed to follow a multivariate circularly symmetric complex Gaussian distribution with zero mean and covariance matrix $\mathbf{C_s}=E\left[\mathbf{s}\mathbf{s}^H\right]$. The elements $[\mathbf{C_s}]_{i,j}=\rho_{i,j}$ represent the correlation between the i-th and j-th source symbols of $\mathbf{s}$. Without loss of generality, we will assume that $\rho_{i,i}=\sigma^2,\forall i$. The probability density function (pdf) of $\mathbf{s}$ is therefore given by

$$p(\mathbf{s})=\frac{1}{\pi^K|\mathbf{C_s}|}\exp\left(-\mathbf{s}^H\mathbf{C_s}^{-1}\mathbf{s}\right). \tag{1}$$

The user symbols are first encoded individually at each transmitter using a specific analog JSCC scheme $\mathrm{f}_k(\cdot):\mathbb{C}\to\mathbb{C}$, and the resulting coded symbols $x_k=\mathrm{f}_k(s_k),k\in\{1,\ldots,K\}$, are then transmitted over the fading MAC to produce the received signal vector $\mathbf{y}\in\mathbb{C}^{N_R}$

$$\mathbf{y}=\sum_{k=1}^{K}\mathbf{h}_k x_k+\mathbf{n}, \tag{2}$$

where $\mathbf{h}_k\in\mathbb{C}^{N_R}$ is the k-th user channel response and $\mathbf{n}=[n_1,\ldots,n_{N_R}]^T\sim\mathcal{N}_{\mathbb{C}}(\mathbf{0},\sigma_n^2\mathbf{I})$ is the AWGN. An individual power constraint is imposed at each transmitter, such that $\mathbb{E}[|x_k|^2]\le P_k,k=1,\ldots,K$. Alternatively, (2) can be rewritten in vector form as

$$\mathbf{y}=\mathbf{H}\mathbf{x}+\mathbf{n} \tag{3}$$

where $\mathbf{H}=[\mathbf{h}_1|\ldots|\mathbf{h}_K]$ and $\mathbf{x}=[x_1,\ldots,x_K]^T$. The vector of encoded symbols is obtained as $\mathbf{x}=\mathrm{f}(\mathbf{s})$, where $\mathrm{f}(\cdot)$ represents the set of all encoding functions, i.e. $\mathrm{f}(\mathbf{s})=[\mathrm{f}_1(s_1),\ldots,\mathrm{f}_K(s_K)]^T$.

A. Real-valued Equivalent Model for Non-linear Mappings

In the ensuing sections, the non-linear mapping functions are applied to complex-valued variables. Some of these mappings will operate independently on the real and imaginary part of the source symbols and, for simplicity, (2) can be transformed into the following real-valued equivalent model

$$\tilde{\mathbf{y}}=\tilde{\mathbf{H}}\,\mathrm{f}(\tilde{\mathbf{s}})+\tilde{\mathbf{n}}=\tilde{\mathbf{H}}\tilde{\mathbf{x}}+\tilde{\mathbf{n}}, \tag{4}$$

where each element $h_{n,k}$ of the original channel matrix $\mathbf{H}$ is transformed into the block

$$[\tilde{\mathbf{H}}]_{n,k}=\begin{pmatrix}\Re\{h_{n,k}\} & -\Im\{h_{n,k}\}\\ \Im\{h_{n,k}\} & \Re\{h_{n,k}\}\end{pmatrix}\quad\begin{matrix}n=1,\ldots,N_R\\ k=1,\ldots,K\end{matrix} \tag{5}$$

the equivalent of vector symbols is $\tilde{\mathbf{s}}=[\Re\{s_1\},\Im\{s_1\},\ldots,\Re\{s_K\},\Im\{s_K\}]^T\in\mathbb{R}^{2K}$, and $\tilde{\mathbf{x}}$ results from applying the mapping operation on the real and

imaginary parts of the source symbols. The vectors $\tilde{\mathbf{y}}$ and $\tilde{\mathbf{n}}$, are also transformed accordingly. After this notation change, $\tilde{\mathbf{s}} \sim \mathcal{N}_{\mathbb{R}}(\mathbf{0}, \mathbf{C}_{\tilde{\mathbf{s}}})$, with $\mathbf{C}_{\tilde{\mathbf{s}}} = \mathbf{C}_{\mathbf{s}} \otimes \frac{1}{2}\mathbf{I}_2$, and $\tilde{\mathbf{n}} \sim \mathcal{N}_{\mathbb{R}}(\mathbf{0}, \frac{\sigma_n^2}{2}\mathbf{I})$

III. Analog JSCC based on Modulo Mappings

Along this work we will assume that MAC users employ modulo mappings to encode their source symbols individually. Modulo mappings have numerous advantages. They allow to design decoding strategies with affordable complexity when the number of users is large, and the encoder is easily adapted to the variations of the channel conditions by optimizing its parameters. In addition, modulo mappings exhibit good performance when analog correlated symbols are transmitted over the MAC using orthogonal signaling [20], [22].

Considering the real-valued equivalent model explained in Section II-A the parametric definition of the modulo mapping function is

$$\mathrm{f}(\tilde{\mathbf{s}}) = \boldsymbol{\Delta} \bmod(\tilde{\mathbf{s}} + \boldsymbol{\alpha}/2, \boldsymbol{\alpha}), \tag{6}$$

where $\tilde{\mathbf{s}}$ is the vector of source symbols in the equivalent model, and $\boldsymbol{\alpha} \in \mathbb{R}^{2K}$ and $\boldsymbol{\Delta} \in \mathbb{R}^{2K\times 2K}$ contain the parameters of the encoding operation. In particular, the k-th element of the vector $\boldsymbol{\alpha}$ corresponds to the modulo argument for the k-th source symbol of $\tilde{\mathbf{s}}$. The optimal values of $\boldsymbol{\alpha}$ depend on the source correlation, the channel response, and the noise variance. The diagonal matrix $\boldsymbol{\Delta}$ preserves the variance of the source symbols after encoding. The k-th diagonal element of this matrix is $\Delta_k = \sqrt{P_k/\omega_k}$, with ω_k the variance of the modulo mapping for given α_k, i.e. $\omega_k = \int_{-\infty}^{\infty} p(s)\,\mathrm{f}_k^2(s)\mathrm{d}s = \int_{-\infty}^{\infty} p(s) \bmod^2(s + \alpha_k/2, \alpha_k)\mathrm{d}s$ where $p(s) = \mathcal{N}(0, \sigma^2)$. Such variance can be expressed in terms of the Gauss error function $Q(\cdot)$ as follows

$$\begin{aligned}\omega_k =& \sigma^2 + \alpha_k^2 \sum_{i=1}^{\infty} i^2 \left(Q\left(n_i\right) - Q\left(m_i\right)\right) \\ &- 2\alpha_k \sqrt{\frac{2\sigma^2}{\pi}} \sum_{i=1}^{\infty} i \left(\exp\left(-m_i^2\right) - \exp\left(-n_i^2\right)\right)\end{aligned} \tag{7}$$

where $m_i = \frac{\alpha_k(2i-1)}{\sqrt{8\sigma^2}}$ and $n_i = \frac{\alpha_k(2i+1)}{\sqrt{8\sigma^2}}$. In this expression, the terms in the sums rapidly converge to zero, and ω_k can be computed accurately with few terms.

At the receiver, an estimate of the source symbols can be obtained from the observed symbols using an appropriate decoding method. In the case of analog communications, the optimal decoding corresponds to the MMSE estimation of the source symbols. However, the resulting integrals can only be computed numerically, and the complexity of this decoding operation is unaffordable even for small number of users. As an alternative, suboptimal decoding methods can be considered like MAP and ML approaches. Unfortunately, the use of modulo functions in these cases leads to non convex optimization problems with multiple local minima. In the following, we show how this limitation can be circumvented by using a piecewise definition of the modulo mapping.

Recall that the mapping function in (6) consists of a set of modulo functions that are individually applied to each component of the source vector $\tilde{\mathbf{s}}$. As observed in Fig. 2, each

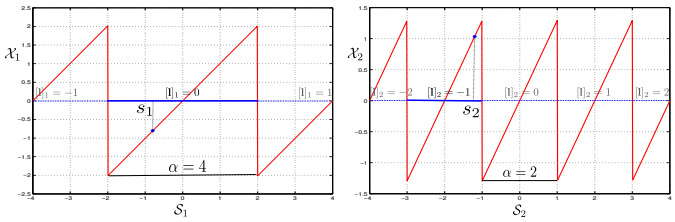

Fig. 2. Example of two modulo functions with parameters $\alpha_1 = 4$ and $\alpha_2 = 2$, respectively, for a transmitted symbol $\mathbf{s} = [-0.8, 1.2]^T$. The corresponding $\mathbf{l}$ for that $\mathbf{s}$ and those α parameters is $\mathbf{l} = [0, 1]^T$.

of these modulo functions splits the source space into a set of non-overlapping intervals such that the corresponding source symbol falls into a unique interval. Notice that the length of the intervals is given by the corresponding component of $\boldsymbol{\alpha}$. Since the source symbols are mapped linearly at each interval, each modulo function in $\mathrm{f}(\cdot)$ can be interpreted as a set of linear functions and, therefore, the mapping in (6) can be expressed in an alternative form as

$$\mathrm{f}(\tilde{\mathbf{s}}) = \boldsymbol{\Delta}(\tilde{\mathbf{s}} - \mathbf{A}\mathbf{l}), \tag{8}$$

where $\mathbf{A} = \mathrm{diag}(\boldsymbol{\alpha})$, and $\mathbf{l} \in \mathbb{Z}^{2K}$ is a vector of integers whose k-th component identifies the interval corresponding to the k-th source symbol of $\tilde{\mathbf{s}}$. Thus, the vector $\mathbf{l}$ explicitly tells us the interval into which each source symbols falls. Mathematically, this vector can be directly determined from the source vector $\tilde{\mathbf{s}}$ as

$$\mathbf{l} = \left\lfloor \mathbf{A}^{-1}\tilde{\mathbf{s}} + \frac{1}{2}\mathbf{I} \right\rfloor.$$

The dependence of $\mathbf{l}$ on $\tilde{\mathbf{s}}$ can be circumvented by redefining the function $\mathrm{f}(\cdot)$ piecewise as

$$\mathrm{f}_i(\tilde{\mathbf{s}}) = \begin{cases} \boldsymbol{\Delta}(\tilde{\mathbf{s}} - \mathbf{A}\mathbf{l}_i) & \mathbf{a}_i \le \tilde{\mathbf{s}} \le \mathbf{b}_i \\ \text{undefined} & \text{otherwise,} \end{cases} \tag{9}$$

where $\mathbf{l}_i \in \mathcal{L}$ represents a particular combination of $2K$ mapping intervals. Notice that $\mathcal{L} \subset \mathbb{Z}^{2K}$ is the set of all integer-valued vectors that represents a feasible combination of mapping intervals. Therefore, the function above is only defined for the vector $\mathbf{l}_i$ that contains the intervals corresponding to the vector of source symbols $\tilde{\mathbf{s}}$. The vectors $\mathbf{a}_i = \mathbf{A}\left(\mathbf{l}_i - \frac{1}{2}\mathbf{1}\right)$ and $\mathbf{b}_i = \mathbf{A}\left(\mathbf{l}_i + \frac{1}{2}\mathbf{1}\right)$ contain the lower and upper limits, respectively, for the sequence of $2N$ intervals given by $\mathbf{l}_i$.

The potential values for the k-th component of $\mathbf{l}$ are determined from the distribution of the k-th source symbol and the corresponding modulo argument $[\boldsymbol{\alpha}]_k$. Feasible values for the zero-mean Gaussian distributed variable $\tilde{\mathbf{s}}$ are not strictly bounded, but we can assume they will fall into an interval such as $(-a\sigma, a\sigma)$, where $a > 0$ is a real value to adjust the confidence of bounding the source values. Hence, an example of definition for $\mathcal{L}$ is the set of all integer-valued vectors $\mathbf{l}$ whose components are

$$\mathcal{L} = \left\{\mathbf{l} \in \mathbb{Z}^{2K} \mid -a\sigma/[\boldsymbol{\alpha}]_k \le [\mathbf{l}]_k \le a\sigma/[\boldsymbol{\alpha}]_k, \forall k \in [1, K]\right\}. \tag{10}$$

In the following, we explore three decoding strategies: ML, MAP and MMSE. The piecewise definition of modulo mappings in (9) is used to reformulate the optimization problem

to find the MAP estimate of the source symbols. The idea is based on obtaining an estimate (candidate) of the source symbols for each feasible combination of intervals, $\mathbf{l}_i \in \mathcal{L}$, and then selecting the estimate that maximizes the MAP criterion from the list of candidates. A similar approach can be followed to obtain the MMSE estimates, although in this case the estimates are calculated by weighting the candidates depending on the probability of each $\mathbf{l}_i$. In addition, a sphere decoder will be employed to lower the complexity of MAP and MMSE methods.

1) ML Decoder: An estimate of the source symbols can be determined using an approach based on a three-step ML decoder for orthogonal channel access [22], [23]. In that scheme, a subset of users directly transmits their source symbols with no coding and the rest uses modulo mappings with a common parameter α, i.e. $\alpha_k = \alpha, \forall k$. In this case, an estimate of the source symbols from the uncoded users is first obtained with the linear MMSE estimator, and then this information helps to recover the symbols of the modulo-mapping users. In this work, we follow the same approach for the case of non orthogonal transmission. First, a linear MMSE estimate for all symbols is obtained from the received symbols as

$$\hat{\mathbf{t}} = \left(\frac{1}{\sigma_n^2}\mathbf{H}^H\mathbf{H} + \mathbf{C}_s^{-1}\right)^{-1}\mathbf{y}. \tag{11}$$

Then, assuming the first user transmits with a large α parameter (uncoded transmission), we estimate the vector of intervals $\mathbf{l}$ corresponding to the transmitted user symbols as

$$\hat{\mathbf{l}} = \left\lfloor \mathbf{A}^{-1}\left(\hat{t}_1\mathbf{1} - \mathbf{\Delta}^{-1}\hat{\mathbf{t}}\right)\right\rceil, \tag{12}$$

where $\hat{t}_1$ represent the first component of $\hat{\mathbf{t}}$. Finally, an estimate of the source symbols is computed as

$$\hat{\mathbf{s}} = \mathbf{\Delta}^{-1}\hat{\mathbf{t}} + \mathbf{A}\hat{\mathbf{l}}. \tag{13}$$

2) MAP Decoder: The MAP estimates of the source symbols are the solutions to the following maximization problem

$$\hat{\mathbf{s}}_{\text{MAP}} = \arg\max_{\tilde{\mathbf{s}}} \; p(\tilde{\mathbf{s}}|\tilde{\mathbf{y}}) = \arg\max_{\tilde{\mathbf{s}}} \; \frac{p(\tilde{\mathbf{y}}|\tilde{\mathbf{s}})p(\tilde{\mathbf{s}})}{p(\tilde{\mathbf{y}})}, \tag{14}$$

where the source pdf $p(\tilde{\mathbf{s}})$ is given by (1), with covariance matrix $\mathbf{C}_{\tilde{\mathbf{s}}}$, and the conditional probability is

$$p(\tilde{\mathbf{y}}|\tilde{\mathbf{s}}) = \left(\pi\sigma_n^2\right)^{-N}\exp\left(-\frac{1}{\sigma_n^2}\|\tilde{\mathbf{y}} - \tilde{\mathbf{H}}\,\mathrm{f}(\tilde{\mathbf{s}})\|^2\right). \tag{15}$$

According to the piecewise definition of the modulo function, this probability can be rewritten in terms of $p(\tilde{\mathbf{y}}|\tilde{\mathbf{s}}) \propto \sum_{i=1}^{|\mathcal{L}|} q_i(\tilde{\mathbf{y}}, \tilde{\mathbf{s}})$ where

$$q_i(\tilde{\mathbf{y}}, \tilde{\mathbf{s}}) = \begin{cases} \exp\left(-\frac{1}{\sigma_n^2}\|\tilde{\mathbf{y}} - \tilde{\mathbf{H}}\,\mathrm{f}_i(\tilde{\mathbf{s}})\|^2\right), & \mathbf{a}_i \le \tilde{\mathbf{s}} \le \mathbf{b}_i \\ 0 & \text{otherwise} \end{cases}, \tag{16}$$

and the normalization factors are omitted for simplicity. Consequently, the function $p(\tilde{\mathbf{s}}|\tilde{\mathbf{y}}) \propto p(\tilde{\mathbf{y}}|\tilde{\mathbf{s}})p(\tilde{\mathbf{s}}) = \sum_i q_i(\tilde{\mathbf{y}}, \tilde{\mathbf{s}})p(\tilde{\mathbf{s}})$ is non-convex and non-differentiable. Notice, however, that the $q_i(\tilde{\mathbf{y}}, \tilde{\mathbf{s}})p(\tilde{\mathbf{s}})$ terms are convex, and hence is possible to find their individual maximum points on $\tilde{\mathbf{s}}$. Then, the MAP estimate can be searched along this set of extreme points.

Indeed, let us define the set of extreme points as $\mathcal{S} = \{\hat{\mathbf{s}}_i, i \in [1, |\mathcal{L}|]\}$, whose elements come from finding the maximum on $\ln(q_i(\tilde{\mathbf{y}}, \tilde{\mathbf{s}})) + \ln(p(\tilde{\mathbf{s}}))$. Replacing the functions $\mathrm{f}_i(\cdot)$ by the corresponding expression in (9), the extreme points $\hat{\mathbf{s}}_i$ can be calculated by solving the optimization problem

$$\begin{aligned} \hat{\mathbf{s}}_i = \arg\min_{\tilde{\mathbf{s}}} \;& \|\tilde{\mathbf{y}} - \tilde{\mathbf{H}}\mathbf{\Delta}(\tilde{\mathbf{s}} - \mathbf{A}\mathbf{l}_i)\|^2 + \frac{\sigma_n^2}{2}\tilde{\mathbf{s}}^T\mathbf{C}_{\tilde{\mathbf{s}}}^{-1}\tilde{\mathbf{s}} \\ s.t. \;& \mathbf{A}\left(\mathbf{l}_i - \frac{1}{2}\mathbf{1}\right) \le \tilde{\mathbf{s}} \le \mathbf{A}\left(\mathbf{l}_i + \frac{1}{2}\mathbf{1}\right), \end{aligned} \tag{17}$$

and the MAP estimate is finally obtained as

$$\hat{\mathbf{s}}_{\text{MAP}} = \arg\max_{\tilde{\mathbf{s}}\in\mathcal{S}} \; p(\tilde{\mathbf{s}}|\tilde{\mathbf{y}}). \tag{18}$$

The problem in (17) can be rewritten in a quadratic form as

$$\begin{aligned} \hat{\mathbf{s}}_i = \arg\min_{\tilde{\mathbf{s}}} \;& \frac{1}{2}\tilde{\mathbf{s}}^T\mathbf{Q}\tilde{\mathbf{s}} - \mathbf{v}_i^T\tilde{\mathbf{s}} \\ s.t. \;& \mathbf{A}\left(\mathbf{l}_i - \frac{1}{2}\mathbf{1}\right) \le \tilde{\mathbf{s}} \le \mathbf{A}\left(\mathbf{l}_i + \frac{1}{2}\mathbf{1}\right). \end{aligned} \tag{19}$$

where $\mathbf{Q} = 2\mathbf{\Delta}^T\tilde{\mathbf{H}}^T\tilde{\mathbf{H}}\mathbf{\Delta} + \sigma_n^2\mathbf{C}_{\tilde{\mathbf{s}}}^{-1}$, and $\mathbf{v}_i = 2\mathbf{\Delta}^T\tilde{\mathbf{H}}^T(\tilde{\mathbf{y}} + \tilde{\mathbf{H}}\mathbf{\Delta}\mathbf{A}\mathbf{l}_i)$.

This problem can be solved by quadratic programming techniques for each candidate vector $\mathbf{l}$. However, if the set of feasible vectors $\mathbf{l}$ is defined as in (10), $|\mathcal{L}|$ increases exponentially with the total number of transmitted symbols N, which makes this direct approach to the MAP estimate infeasible for large number of users.

3) MMSE Decoder: The optimal decoder according to the Mean Squared Error (MSE) distortion criteria is the MMSE decoder given by

$$\hat{\mathbf{s}} = \mathbb{E}(\tilde{\mathbf{s}}|\tilde{\mathbf{y}}) = \int \tilde{\mathbf{s}}p(\tilde{\mathbf{s}}|\tilde{\mathbf{y}})d\tilde{\mathbf{s}} \tag{20}$$

Using the piecewise definition of the conditional probability in (16), the term $p(\tilde{\mathbf{s}}|\tilde{\mathbf{y}})$ can be expressed as $p(\tilde{\mathbf{s}}|\tilde{\mathbf{y}}) \propto \sum_i r_i(\tilde{\mathbf{y}}, \tilde{\mathbf{s}})$, where

$$r_i(\tilde{\mathbf{y}}, \tilde{\mathbf{s}}) \propto \begin{cases} \phi_i t(\tilde{\mathbf{s}}|\boldsymbol{\mu}_i, \mathbf{\Sigma}), & \mathbf{a}_i \le \tilde{\mathbf{s}} \le \mathbf{b}_i \\ 0 & \text{otherwise} \end{cases}, \tag{21}$$

with $t(\tilde{\mathbf{s}}|\boldsymbol{\mu}_i, \mathbf{\Sigma}) = \left((2\pi)^{2N}|\mathbf{\Sigma}|\right)^{-1/2}\exp\left(-\frac{1}{2}\left(\tilde{\mathbf{s}} - \boldsymbol{\mu}_i\right)^T\mathbf{\Sigma}^{-1}\left(\tilde{\mathbf{s}} - \boldsymbol{\mu}_i\right)\right)$ and

$$\phi_i = \exp\left(-\frac{1}{2}\left(\sigma_n^{-2}\|\tilde{\mathbf{y}} - \tilde{\mathbf{H}}\mathbf{\Delta}\mathbf{A}\mathbf{l}_i\|^2 - \boldsymbol{\mu}_i^T\mathbf{\Sigma}^{-1}\boldsymbol{\mu}_i\right)\right) \tag{22}$$

$$\boldsymbol{\mu}_i = \frac{1}{\sigma_n^2}\mathbf{\Sigma}\mathbf{\Delta}^T\tilde{\mathbf{H}}^T(\tilde{\mathbf{y}} + \tilde{\mathbf{H}}\mathbf{\Delta}\mathbf{A}\mathbf{l}_i), \tag{23}$$

$$\mathbf{\Sigma} = \left(\frac{1}{\sigma_n^2}\mathbf{\Delta}^T\tilde{\mathbf{H}}^T\tilde{\mathbf{H}}\mathbf{\Delta} + \mathbf{C}_{\tilde{\mathbf{s}}}^{-1}\right)^{-1}. \tag{24}$$

A more detailed explanation of this transformation is provided in Appendix A. As observed, using the piecewise definition of the modulo function, the integral in (20) can be decomposed into a sum of terms weighted by the corresponding factor ϕ_i.

Since the function $t(\tilde{\mathbf{s}}|\boldsymbol{\mu}_i, \boldsymbol{\Sigma})$ is the pdf of a multivariate Gaussian with mean $\boldsymbol{\mu}_i$ and covariance matrix $\boldsymbol{\Sigma}$, the MMSE estimation of the source symbols is calculated as

$$\hat{\mathbf{s}}_{\text{MMSE}} = \frac{\sum_i \phi_i \Theta(\mathbf{a}_i, \mathbf{b}_i; \boldsymbol{\Sigma}, \boldsymbol{\mu}_i)}{\sum_i \phi_i \Phi(\mathbf{a}_i, \mathbf{b}_i; \boldsymbol{\Sigma}, \boldsymbol{\mu}_i)} \tag{25}$$

where $\Theta(\mathbf{a}_i, \mathbf{b}_i; \boldsymbol{\Sigma}, \boldsymbol{\mu}_i) = \int_{\mathbf{a}_i}^{\mathbf{b}_i} \tilde{\mathbf{s}} t(\tilde{\mathbf{s}}|\boldsymbol{\mu}_i, \boldsymbol{\Sigma}) \mathrm{d}\tilde{\mathbf{s}}$ is the mean of a multivariate Gaussian truncated to the orthant given by the limits $\mathbf{a}_i$ and $\mathbf{b}_i$, and $\Phi(\mathbf{a}_i, \mathbf{b}_i; \boldsymbol{\Sigma}, \boldsymbol{\mu}_i) = \int_{\mathbf{a}_i}^{\mathbf{b}_i} t(\tilde{\mathbf{s}}|\boldsymbol{\mu}_i, \boldsymbol{\Sigma}) \mathrm{d}\tilde{\mathbf{s}}$ is the orthant cumulative distribution of a multivariate Gaussian variable.

Note that (25) provides a lower complexity solution to the general MMSE estimation problem, but it also turns out to be infeasible when the number of users is large for two reasons. First, the orthant cumulative distribution of a Gaussian variable cannot be efficiently approximated for dimensions larger than three, and techniques such as importance sampling should be used to approximate it [25]. The other drawback is shared with the MAP estimator, and it is related to the exponentially growing size of $\mathcal{L}$ when the number of users grows. In the ensuing section, this problem will be addressed with the help of a sphere decoder that will allow us to limit the number of feasible $\mathbf{l}$ vectors in the set $\mathcal{L}$ as the number of users increases, while ensuring that the optimal $\mathbf{l}$ is contained in it.

IV. Sphere Decoder for Modulo Mappings

The direct implementation of the MMSE decoder from (25) is computationally costly. Nevertheless, the examination of (25) provides insight in the behavior of the MMSE estimator. First, the MMSE estimator results from a weighted sum of evaluations $\Theta(\mathbf{a}_i, \mathbf{b}_i; \boldsymbol{\Sigma}, \boldsymbol{\mu}_i)$ at different points. This function is the average of a Gaussian variable bounded to a region, and its evaluation gives values in the interval $\mathbf{a}_i \Phi(\mathbf{a}_i, \mathbf{b}_i; \boldsymbol{\Sigma}, \boldsymbol{\mu}_i) \leq \Theta(\mathbf{a}_i, \mathbf{b}_i; \boldsymbol{\Sigma}, \boldsymbol{\mu}_i) \leq \mathbf{b}_i \Phi(\mathbf{a}_i, \mathbf{b}_i; \boldsymbol{\Sigma}, \boldsymbol{\mu}_i)$. Since these values are bounded, an approximation of the estimator can be obtained by evaluating $\Theta(\mathbf{a}_i, \mathbf{b}_i; \boldsymbol{\Sigma}, \boldsymbol{\mu}_i)$ only when the weights ϕ_i take large values.

Note also that for high Signal-to-Noise Ratio (SNR) values, the function $\Theta(\mathbf{a}_i, \mathbf{b}_i; \boldsymbol{\Sigma}, \boldsymbol{\mu}_i) \approx \hat{\mathbf{s}}_i \Phi(\mathbf{a}_i, \mathbf{b}_i; \boldsymbol{\Sigma}, \boldsymbol{\mu}_i)$, with $\hat{\mathbf{s}}_i$ the solution to the partial MAP problem posed in (17). On the other hand, the MAP and MMSE solutions converge in the high SNR region. This provides the intuition that the distribution of the weights ϕ_i will peak around the solution $\hat{\mathbf{s}}_i$ corresponding to the optimal $\mathbf{l}_i$, and this search for the large ϕ_i will likely provide good candidates for the MAP estimator.

The problem of estimating the source symbols can hence be reformulated as finding those vectors $\mathbf{l}_i$ whose corresponding weight ϕ_i is significant. The search of the candidates $\mathbf{l}_i$ can be done by selecting only those weights ϕ_i larger than a given threshold T, i.e.,

$$\phi_i = \exp\left(-\frac{1}{2}\left(\sigma_n^{-2}\|\tilde{\mathbf{y}} + \tilde{\mathbf{H}}\boldsymbol{\Delta}\mathbf{A}\mathbf{l}_i\|^2 - \boldsymbol{\mu}_i^T \boldsymbol{\Sigma}^{-1} \boldsymbol{\mu}_i\right)\right) > T. \tag{26}$$

This problem can be equivalently formulated as the search for the candidate vectors that make the exponent below some radius R. Taking this into account, an alternative definition of the set $\mathcal{L}$ is $\mathcal{L}_R = \{\mathbf{l} \in \mathbb{Z}^{2K} | h(\mathbf{l}) < R\}$, with

$$h(\mathbf{l}) = \frac{1}{2}\left(\sigma_n^{-2}\|\tilde{\mathbf{y}} + \tilde{\mathbf{H}}\boldsymbol{\Delta}\mathbf{A}\mathbf{l}\|^2 - \boldsymbol{\mu}_\mathbf{l}^T \boldsymbol{\Sigma}^{-1} \boldsymbol{\mu}_\mathbf{l}\right), \tag{27}$$

and

$$\boldsymbol{\mu}_\mathbf{l} = \frac{1}{\sigma_n^2} \boldsymbol{\Sigma} \boldsymbol{\Delta}^T \tilde{\mathbf{H}}^T (\tilde{\mathbf{y}} + \tilde{\mathbf{H}}\boldsymbol{\Delta}\mathbf{A}\mathbf{l}). \tag{28}$$

The original problem of estimating the analog source symbols is hence reduced to look for the most likely discrete vectors $\mathbf{l}$ used during the transmission. In the literature, different approaches have been proposed to solve this kind of problems and one of the most appealing is the sphere decoder, originally proposed to detect digital signals in MIMO transmissions [26]. Notice that the sphere decoder is a general strategy to search for the shortest vector in a lattice, and the modulo mapping can actually be interpreted as a lattice.

To apply the sphere decoder, (27) must be rewritten as

$$h(\mathbf{l}) = (\mathbf{l} + \mathbf{l}_o)^T \boldsymbol{\Lambda} (\mathbf{l} + \mathbf{l}_o), \tag{29}$$

where

$$\boldsymbol{\Lambda} = \frac{1}{2}\mathbf{A}^T \boldsymbol{\Delta}^T \tilde{\mathbf{H}}^T \left(\sigma_n^2 \mathbf{I} + \tilde{\mathbf{H}}\boldsymbol{\Delta}\mathbf{C}_{\tilde{\mathbf{s}}}\boldsymbol{\Delta}^T \tilde{\mathbf{H}}^T\right)^{-1} \tilde{\mathbf{H}}\boldsymbol{\Delta}\mathbf{A}, \tag{30}$$

is the matrix that represents the lattice that summarizes the effecs of the channel and the modulo mapping, and

$$\mathbf{l}_o = (\mathbf{A}^T \boldsymbol{\Delta}^T \tilde{\mathbf{H}}^T \tilde{\mathbf{H}} \boldsymbol{\Delta}\mathbf{A})^{-1} \mathbf{A}^T \boldsymbol{\Delta}^T \tilde{\mathbf{H}}^T \tilde{\mathbf{y}}$$

represents the center of the sphere where candidates for $\mathbf{l}$ will be searched for. Appendix B details the steps of this transformation.

The search of the $\mathbf{l}$ vectors that make $h(\mathbf{l})$ to be below some radius is performed by means of the Cholesky decomposition $\boldsymbol{\Lambda} = \mathbf{L}\mathbf{L}^T$ and iteratively obtaining a feasible range of values for each component of $\mathbf{l}$ that satisfy the considered radius given the previous components. Following an approach similar to [26], at the n-th iteration the sphere decoder will select the values for the n-th component of $\mathbf{l}$ that fall into the interval

$$\underbrace{[\mathbf{l}_o]_n - d_n - \frac{\sqrt{4R^2 - c_n}}{[\mathbf{L}]_{nn}}}_{I_n(\mathbf{l})} \leq [\mathbf{l}]_n \leq \underbrace{[\mathbf{l}_o]_n - d_n + \frac{\sqrt{4R^2 - c_n}}{[\mathbf{L}]_{nn}}}_{O_n(\mathbf{l})} \tag{31}$$

with

$$d_n = \sum_{i=1}^{n-1} \frac{[\mathbf{L}]_{n,i}}{[\mathbf{L}]_{n,n}} \left([\mathbf{l}]_i + [\mathbf{l}_o]_i\right),$$

$$c_n = c_{n-1} + \left(\sum_{i=1}^{n-1} [\mathbf{L}]_{n-1,i} ([\mathbf{l}]_i + [\mathbf{l}_o]_i)\right)^2$$

where $c_0 = 0$. In this work, the set of vectors $\mathbf{l}$ is built recursively as $\mathcal{L}_R = \mathcal{L}_R^{2N}$, where

$$\mathcal{L}_R^n = \{\mathbf{l} \in \mathbb{Z}^n | \mathbf{l} = [\mathbf{m}^T m]^T, I_n(\mathbf{m}) \leq m \leq O_n(\mathbf{m}), \forall \mathbf{m} \in \mathcal{L}_R^{n-1}\}, \quad \mathcal{L}_R^0 = \tag{32}$$

Using the sphere decoder to build the set $\mathcal{L}$ makes the MAP estimation affordable for large number of users. In addition, it reduces the complexity of the MMSE decoder in (25),

although the practical implementation of this strategy is still only feasible for a small number of source symbols due to the complexity of the evaluation of the Θ and Φ functions. Finally, the distribution of the weights ϕ_i also determines the distortion of the MMSE estimator: for flatter distributions, the MSE should be larger. On the other hand, when one weight is significantly larger than the others, the MSE will be well approximated by the variance of the main lobe of the posterior distribution, i.e., by the matrix $\mathbf{\Sigma}$.

A. Radius Selection

An important issue when using the sphere decoder is to ensure it provides a set $\mathcal{L}_R$ that includes those vectors $\mathbf{l}$ with a significant weight. This requires an adequate optimization of the radius employed at the decoding step. Let us assume a specific vector $\hat{\mathbf{l}}$ is transmitted and its value is known at the receiver. Using $\tilde{\mathbf{y}} = \tilde{\mathbf{H}}\mathbf{\Delta}(\tilde{\mathbf{s}} - \mathbf{A}\hat{\mathbf{l}}) + \tilde{\mathbf{n}}$, it is possible to rewrite the first term in (27) as $\tilde{\mathbf{y}} + \tilde{\mathbf{H}}\mathbf{\Delta}\mathbf{A}\hat{\mathbf{l}} = \tilde{\mathbf{H}}\mathbf{\Delta}\tilde{\mathbf{s}} + \tilde{\mathbf{n}} = \mathbf{z}$. Replacing this expression in (27), and using the definition (23) for the $\boldsymbol{\mu}_i$ values, the metric for the sphere decoder can be rewritten as

$$\begin{aligned} h(\hat{\mathbf{l}}) =& \frac{1}{2}\left(\sigma_n^{-2}\|\mathbf{z}\|^2 - \sigma_n^{-4}\mathbf{z}^T\tilde{\mathbf{H}}\mathbf{\Delta}\mathbf{\Sigma}\mathbf{\Delta}^T\tilde{\mathbf{H}}^T\mathbf{z}\right) \\ =& \frac{1}{2}\mathbf{z}^T\left(\sigma_n^{-2}\mathbf{I} - \sigma_n^{-4}\tilde{\mathbf{H}}\mathbf{\Delta}\mathbf{\Sigma}\mathbf{\Delta}^T\tilde{\mathbf{H}}^T\right)\mathbf{z} \\ =& \frac{1}{2}\mathbf{z}^T\left(\sigma_n^2\mathbf{I} + \tilde{\mathbf{H}}\mathbf{\Delta}\mathbf{C}_{\tilde{\mathbf{s}}}\mathbf{\Delta}^T\tilde{\mathbf{H}}^T\right)^{-1}\mathbf{z} \end{aligned} \tag{33}$$

Given that $E(\mathbf{z}\mathbf{z}^T) = \sigma_n^2\mathbf{I} + \tilde{\mathbf{H}}\mathbf{\Delta}\mathbf{C}_{\tilde{\mathbf{s}}}\mathbf{\Delta}^T\tilde{\mathbf{H}}^T = \mathbf{Z}$, the exponent for $\hat{\mathbf{l}}$ follows a distribution $\mathbf{z}^T\mathbf{Z}^{-1}\mathbf{z} \sim \chi^2_{2K}$. Since we are assuming that the mapping is designed to achieve the minimum weight ϕ for this $\hat{\mathbf{l}}$, it is safe to assume that the radius must be at least

$$R \geq g_{2K}^{-1}(\tau)/2, \tag{34}$$

with $g_k(r) = P(\chi_k^2 < r)$ the cumulative distribution function of a chi-squared variable with k degrees of freedom, and $g_k^{-1}(\cdot)$ its inverse function. In this case, $\tau \in [0, 1]$ is a parameter to adjust the likelihood of obtaining a $\mathcal{L}_R \neq \emptyset$. We have checked experimentally that the criterion (34) provides good candidates for $\mathbf{l}$ when $\tau \geq 1 - 10^{-5}$. If no candidates are found for a given τ, decoding can be repeated with a larger parameter until solutions are found.

B. Design of Mapping Parameters

The optimization of the user mappings is fundamental to minimize the signal distortion. In the case of modulo mappings, two parameter matrices, $\mathbf{A}$ and $\mathbf{\Delta}$, are involved in the optimization procedure, although the values of $\mathbf{\Delta}$ can actually be determined from $\mathbf{A}$ and from the user power constraints, as shown in (7). An adequate tradeoff for α_k is essential to achieve the lowest possible distortion. On the one hand, a lower α_k implies a larger value for Δ_k and, as a consequence, the distortion is reduced since the error covariance in (24) explicitly depends on $\mathbf{\Delta}$. On the other hand, if α_k is too small, the sphere decoder can break down due to the large number of candidate vectors with similar weight.

Given that the optimal parameters are difficult to obtain from an analytical expression due to the nature of the modulo functions, we propose two optimization strategies depending on whether the channel information is available. To design the parameters α_k, we first define a lower bound according to the systematic error of the encoder, and then study the influence of the channel to enhance the optimization.

1) Source Correlation Criterion: In this strategy, we determine the α_k values from the information of the sources distribution. Specifically, α_k is selected according to the conditional variance $\sigma^2_{k|k-1}$ to guarantee no ambiguities in the mapping operation. This choice lies on the iterative nature of the analog encoder based on modulo functions. Ambiguities on the encoding step can be prevented by using a large α for the first user, while the next users can lower their α values successively without creating ambiguities that break down the decoding procedure.

Let $\mathbf{s}_k = [\tilde{s}_1, \ldots, \tilde{s}_k]^T$ be the vector that stacks the source symbols up to the k-th symbol, and $\mathbf{D}_k = \mathbb{E}[\mathbf{s}_k\mathbf{s}_k^T]$ such that

$$\mathbf{D}_k = \begin{pmatrix} \mathbf{D}_{k-1} & \mathbf{d}_k \\ \mathbf{d}_k^T & \sigma^2 \end{pmatrix}, \tag{35}$$

where σ^2 is the variance of the k-th source symbol, and $\mathbf{d}_k = \mathbb{E}[s_k\mathbf{s}_{k-1}^T]$ the covariance of the k-th source symbol with the $k-1$ previous symbols. In this case, considering that $\mathbf{s}_k$ is Gaussian, the variance of the k-th source symbol conditioned to the previous symbols is given by $\sigma^2_{k|k-1} = \sigma^2 - \mathbf{d}_k^T\mathbf{D}_{k-1}^{-1}\mathbf{d}_k$.

A suitable choice can be $\alpha_k = 2\sigma_{k|k-1}\varrho$ with ϱ a parameter to adjust the likelihood of missing the right modulo mapping cut. We have found that values around $\varrho = 6$ provide good α_k parameters.

2) Channel State Criterion: Although the method above provides a lower bound for practical values of α_k, it can be optimistic depending on the channel conditions. With the help of the structure of the sphere decoder, a tighter bound for α_k can be defined. Recall that the lattice where the feasible $\mathbf{l}$ are searched for is defined by the matrix $\mathbf{\Lambda}$ in (30), which depends on the parameter matrices $\mathbf{A}$ and $\mathbf{\Delta}$. We can define an alternative lattice as $\bar{\mathbf{\Lambda}} = \mathbf{A}^{-1}\mathbf{\Lambda}\mathbf{A}^{-1}$, and a decomposition $\bar{\mathbf{\Lambda}} = \bar{\mathbf{L}}\bar{\mathbf{L}}^T$. The expression in (29) can now be written as

$$h(\mathbf{l}) = (\mathbf{l} + \mathbf{l}_o)^T\mathbf{A}^T\bar{\mathbf{L}}\bar{\mathbf{L}}^T\mathbf{A}(\mathbf{l} + \mathbf{l}_o), \tag{36}$$

and $\mathbf{A}$ can be adjusted to shape the lattice. The dependence of $\mathbf{\Delta}$ on $\mathbf{A}$ can be addressed by using an iterative algorithm where $\mathbf{\Delta}$ is first initialized as $\mathbf{\Delta} = \mathbf{P}$, the parameters in $\mathbf{A}$ are computed, and the new values for $\mathbf{\Delta}$ are then obtained according to (7). In the next iteration, these values are used to recalculate the lattice and to update $\mathbf{A}$.

Recalling that we are interested in generating a set $\mathcal{L}_R$ as small as possible for a given radius R, matrix $\mathbf{A}$ can be defined so that variations in any component of $\mathbf{l}$ cause large variations in the metric $h(\mathbf{l})$. In the n-th iteration of the sphere decoder,

the metric can be written as

$$h_n(\mathbf{l}) = \sum_{j=1}^{n-1}\left(\sum_{k=1}^{j}\alpha_k L_{j,k}(l_k + l_{o,k})\right)^2 + \underbrace{\left(\sum_{k=1}^{n-1}\alpha_k L_{n,k}(l_k + l_{o,k}) + \alpha_n L_{n,n}(l_n + l_{o,n})\right)^2}_{g_n(l_n)}. \quad (37)$$

It can be seen that α_n only affects the metric with the variations on l_n, the n-th component in $\mathbf{l}$. Therefore, a feasible criterion to choose α_n is

$$|g_n(l_n) - g_n(l_n + 1)| \geq S, \quad (38)$$

where S represents the minimum desired distance between contiguous points in the n-th dimension of the lattice. From (37) it is obtained that

$$|g_n(l_n) - g_n(l_n + 1)| = \alpha_n^2 L_{n,n}^2 + 2g_n(l_n)\alpha_n L_{n,n} \geq S. \quad (39)$$

Notice that $h_n(\mathbf{l}) \approx 0$ when $\mathbf{l} = \hat{\mathbf{l}}$ corresponds to the truly transmitted symbol. As a consequence, $g_n(\hat{l}_n) \approx 0$ and the determination of the mapping parameter simplifies to $\alpha_n \geq \frac{\sqrt{S}}{L_{n,n}}$.

V. Simulation Results

In this section, the results of several computer experiments are presented to illustrate the performance of the proposed analog JSCC scheme for different MAC scenarios.

Source symbols are assumed to be complex-valued circularly-symmetric zero-mean multivariate Gaussian with covariance matrix $\mathbf{C_s}$. Let us consider that these symbols are normalized, i.e., $\rho_{i,i} = 1 \quad \forall i = 1, \ldots, K$, and two different correlation models: 1) the correlation between all the source symbols is the same, thus $\rho_{i,j} = \rho \quad \forall i \neq j$; and 2) the correlation between the i-th and j-th source symbols is modeled as $\rho_{i,j} = \rho^{|i-j|}, \forall i, j$. The first situation is referred to as equal source correlation and the second one as exponential source correlation. The user symbols are encoded individually at each transmitter by using the modulo mappings described in Section III. The optimal values of the mapping parameters are obtained according to the strategies explained in Section IV-B, depending on whether CSI is available at transmitters. After the encoding step, the resulting symbols are transmitted over a Rayleigh fading MAC with a matrix response $\mathbf{H} \in \mathbb{C}^{N_R \times K}$. At the receiver, estimates of the source symbols are calculated with the help of the sphere decoder. Finally, the expected sum-distortion between the source and decoded symbols is computed. In general, we address the symmetric case where the power constraints for all users are equal, i.e., $P = P_i \ \forall i = 1, \ldots, K$. When considering different power constraints for the MAC users, the power model will be described explicitly. We will also focus on scenarios with $K \leq N_R$, i.e., the number of users does not exceed the number of receive antennas.

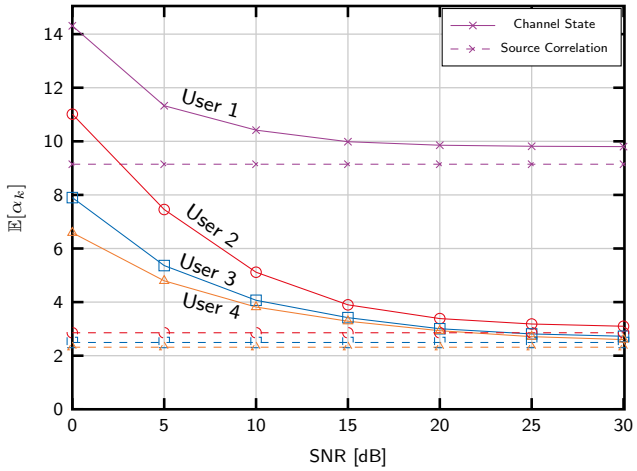

Fig. 3. Average α_k values with respect to SNR in a scenario with $K = 4$, $N_R = 4$ and $\rho = 0.95$. Solid lines corresponds to values of α_k obtained by Channel State optimization, and dashed lines to Source Correlation optimization.

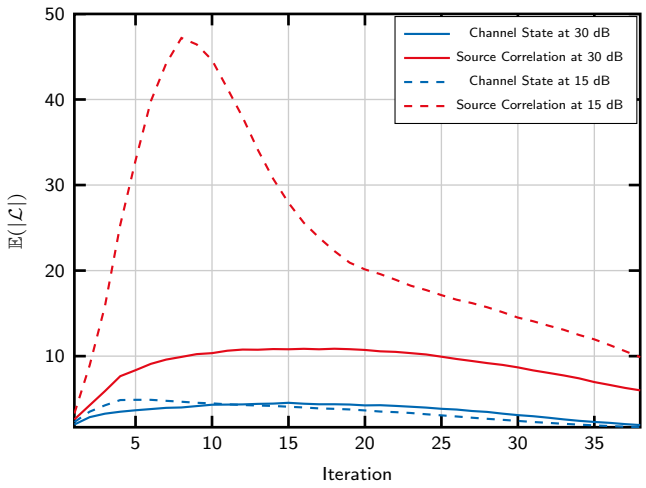

Fig. 4. Cardinality of the set of feasible $\mathbf{l}$ vectors with the two optimization strategies for $K = 20$, $N_R = 20$ and $\rho = 0.95$.

A. Optimization of the Analog JSCC System

As commented, two different criteria will be considered to optimize the parameters of the user mappings: the source correlation criterion and the channel state criterion.

Fig. 3 shows the average value of the parameters α_k obtained with these two optimization strategies for different SNRs in a scenario with $K = 4$, $N_R = 4$ and $\rho = 0.95$ using the equal correlation model. As observed, when using the channel state criterion, the α_k values decrease for all users as the SNR increases. In addition, this strategy shows that one of the MAC users should transmit its data with a large α_k to avoid ambiguities, while the last users can use lower α_k values given that more information from the previously decoded symbols is available. When the optimization is based on the source correlation, the same α_k is obtained for all SNRs. However, the values calculated according to this criterion are usually optimistic for adverse channel realizations.

Another important issue is the computational cost of the decoding operation. The complexity of MAP and MMSE estimators depend on the cardinality of the set of $\mathbf{l}$ vectors that

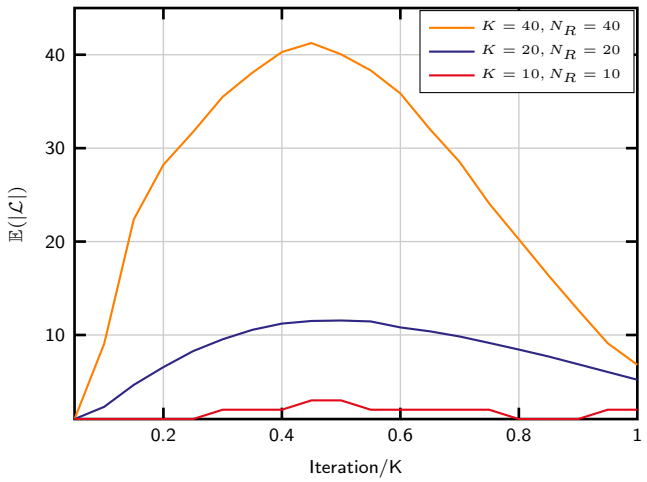

Fig. 5. Cardinality of the set of feasible $\mathbf{l}$ vectors for different number of users and with $\rho = 0.95$.

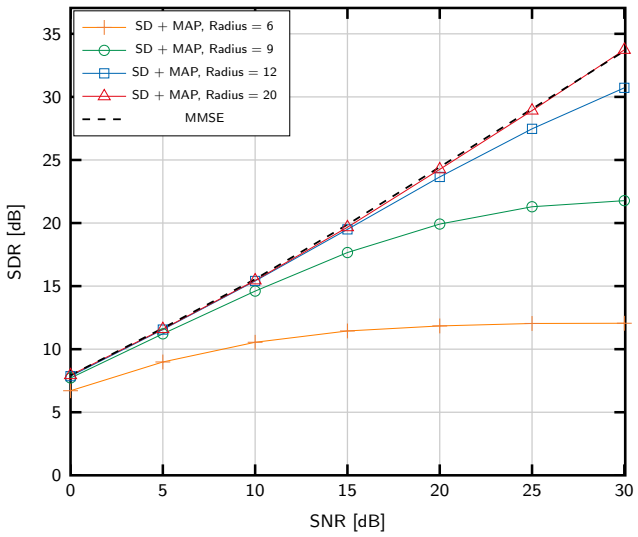

Fig. 6. Performance of modulo mappings with the optimal MMSE estimator and with the MAP strategy depending on the radius of the sphere decoder for $K = 2$, $N_R = 4$ and $\rho = 0.95$.

the sphere decoder obtains. The evolution of the number of $\mathbf{l}$ candidates that falls into the decoding sphere is shown in Fig. 4 for the two optimization strategies in a $K = 20$, $N_R = 20$ scenario with $\rho = 0.95$. As observed, the size of the set of candidate vectors is smaller along all iterations of the decoding algorithm when using the channel state criterion, since the parameters α_k are selected depending on each channel realization. The sphere decoder with a parameter optimization based on the source correlation criterion provides larger number of candidate vectors and, consequently, the computational cost of the decoding operation is also higher. The increase of the set size is more significant as the SNR decreases, since the values of α_k are in general too optimistic.

Fig. 5 shows the evolution of the number of $\mathbf{l}$ candidates depending on the number of MAC users K with the channel state optimization strategy for SNR $= 30$ dB and $\rho = 0.95$. As observed, the number of candidate vectors increases as the number of users grows. Unlike the general case without the sphere decoder, this increase is not dramatic, and the decoding operation is still affordable.

B. Performance Evaluation

Analog communication systems are often designed to transmit and recover the source information with the lowest possible distortion and, therefore, their performance is usually measured in terms of the Signal-to-Distortion Ratio (SDR) with respect to the channel SNR. Since we focus on the sum-distortion, and considering the MSE as distortion criteria, the SDR is calculated as

$$\text{SDR[dB]} = 10\log_{10}(1/\xi), \tag{40}$$

where the term $\xi = \frac{1}{K}\sum_{k=1}^{K}\mathbb{E}\left[\|\hat{s}_k - s_k\|^2\right]$ is the average sum-MSE between the source and the estimated symbols.

The theoretical optimal performance of analog communications is given by the optimal cost-distortion tradeoff, referred to as the Optimum Performance Theoretically Attainable (OPTA). This bound is in general unknown when transmitting correlated data over the MAC. In this paper, we consider an upper bound based on the source-channel separation to illustrate the theoretical optimal performance. The steps to determine this bound are described in Appendix C.

In the first experiment, we test the performance of the proposed sphere decoder to lower the complexity of MAP decoding. The evolution of the system performance depending on the radius in the sphere decoder is shown in Fig. 6, using parameters obtained by the channel state optimization. The performance curve corresponding to the optimal MMSE method and the separation bound calculated according to (58) are also included for comparison. A scenario with $K = 2$ and $N_R = 4$ is chosen since the optimal MMSE decoding is unfeasible for larger number of users. We also focus on the equal source correlation model with variance $\sigma^2 = 1$ and a correlation factor $\rho = 0.95$. Hence, $\mathbf{C_s} = [1\ 0.95;\ 0.95\ 1]$. As observed, the system performance gradually improves as the radius of the sphere decoder becomes larger, until it converges to the MMSE curve when the radius is $R = 20$. From these results, we can conclude that: 1) MAP strategy is able to achieve the performance of the MMSE decoding for all SNRs, and 2) the use of the sphere decoder does not penalize the system performance as long as the radius is properly selected to include those solutions with significant weight. In addition, the gap between the best SDR curve for the MAP strategy and the separation bound is relatively small, since it goes from 2 dB for low SNRs to less than 4 dB for high SNRs. It is worth noting that in this scenario with two users the bound is exact, since the constraints on the individual capacities are employed to determine the bound (see Appendix C).

Next, we consider a scenario where $K = 4$ users transmit multivariate Gaussian symbols with the same correlation factor $\rho = 0.95$. The parameters are optimized according to the channel state criterion. At the receiver, three decoding methods are considered: 1) MMSE with sphere decoder, 2) MAP with sphere decoder and 3) ML decoding as in [23] for lattice mappings extended to non-orthogonal transmissions. The first two approaches use the sphere decoder to lower the complexity of the decoding operation.

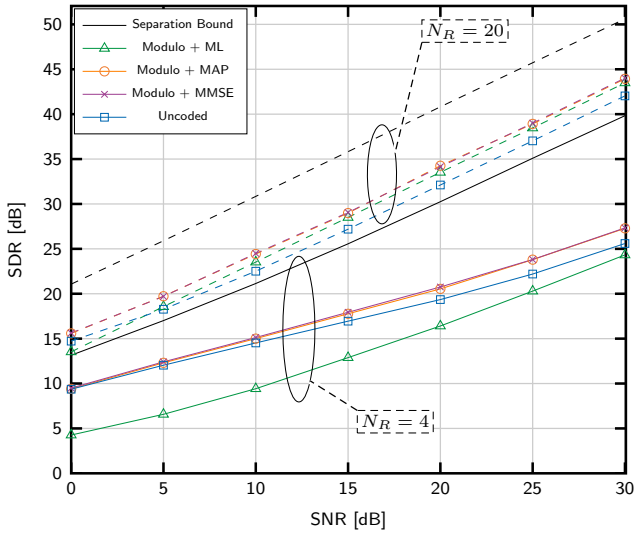

Fig. 7. SDR against SNR with different decoders for $K = 4$ and $\rho = 0.95$. Two different number of receive antennas, $N_R = 4$ and $N_R = 20$, are considered.

Fig. 7 shows the performance of the analog JSCC system for $N_R = 4$ and $N_R = 20$ receive antennas with the three decoding approaches. The performance of the uncoded scheme and the upper bound with separation given by (58) are also plotted for comparison. On the one hand, the performance provided by MAP and MMSE decoding is very similar, with only a slight gain in SDR with MMSE decoding. Also, the ML decoder cannot reach the performance of the MAP and MMSE when the number of receive antennas is low because this decoding algorithm is designed to work under orthogonal access to the channel. When the number of antennas increases, the channels observed by each user are more orthogonal to each other, and hence the ML is able to overcome the uncoded scheme. However, it is still below the performance obtained with the MAP. On the other hand, the analog JSCC scheme using modulo mappings outperforms the uncoded transmission for all the range of SNRs, although the SDR gain is more significant for high SNRs where this gain is almost 2 dBs for $N_R = 4$ and $N_R = 20$.

When $N_R = 4$ the gap between the performance of the modulo mappings and the separation upper bound grows as the SNR increases (from 3.5 dB at SNR $= 0$ dB to 12 dB at SNR $= 30$ dB). This behaviour is not observed for $N_R = 20$ where the slope of the performance curve is similar to that of the separation bound. This is due to intrinsic limitations of the modulo mappings. Although the SNR increases, it is not possible to lower the values of α_k below a certain threshold, given by the source correlation, without creating ambiguities at the decoding operation. Recall that the separation bound for $K > 2$ is plotted as reference. This bound is actually higher than the real bound since the constraints for the individual rates are disregarded. Moreover, the separation bound is calculated under the assumption of infinite block length for the source and channel encoders.

We next move to scenarios with more MAC users where the use of the sphere decoder is essential. Fig. 8 shows the performance of the analog JSCC system with modulo encoding

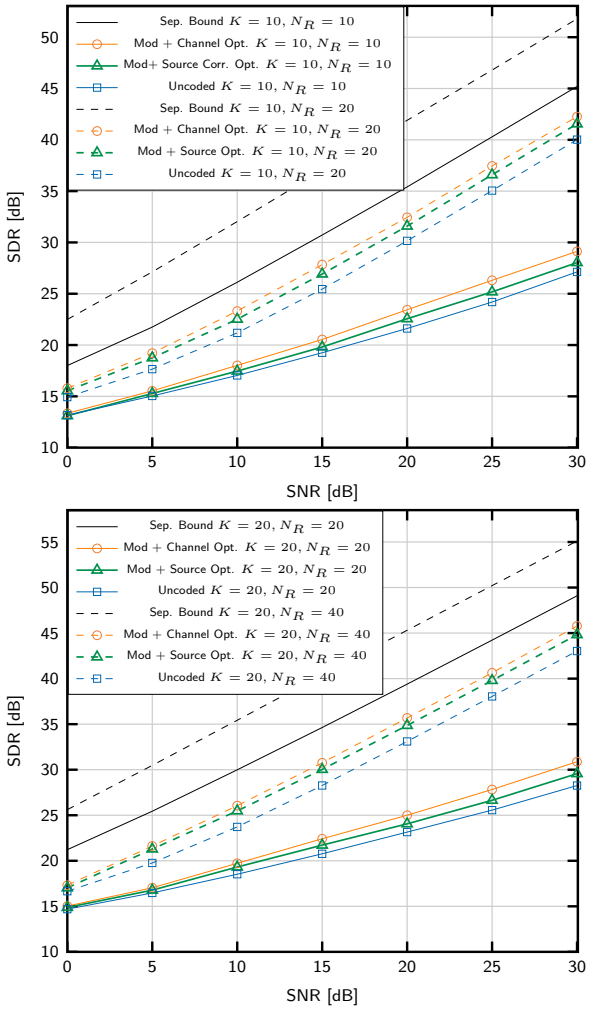

Fig. 8. Performance curves obtained with modulo mappings and uncoded transmission for $K = N_R = 10$ and $K = 10$ $N_R = 20$ (left side), and for $K = N_R = 20$ and $K = 20$ $N_R = 40$ scenarios, considering a correlation factor $\rho = 0.95$ in both cases.

and MAP decoding with sphere decoder for $K = 10$ users (left hand) and $K = 20$ users (right hand). In both cases, two different situations are evaluated: 1) $N_R = K$ and 2) $N_R = 2K$. Like in the previous case, we consider the source model with equal correlation $\rho = 0.95$. The mapping parameters are optimized according to the two proposed strategies: source correlation and channel state criteria. The SDR curves obtained with both optimization strategies are also plotted in Fig. 8. Again, the performance of the uncoded scheme and the upper bounds with separation are included for comparison.

As observed in both figures, when considering scenarios with larger number of users the modulo mappings present a similar behaviour to the case of $N_R = 4$ antennas and $K = 4$ users. On one hand, these mappings outperform the uncoded scheme for the whole range of SNRs. The performance gain grows as the SNR is higher and it also increases as the number of users grows. The gap between the modulo mapping and the uncoded scheme was slightly below 2 dB for $K = 4$ and high SNRs, while this difference increases up to 2.5 dB for $K = 10$ users and almost 3 dB for $K = 20$ users. For the considered correlation model, lower values for the

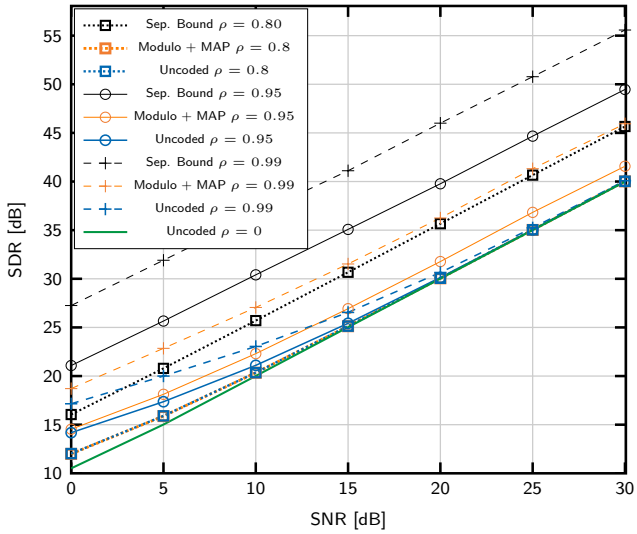

Fig. 9. Performance of uncoded and modulo mappings for $K = 10$ and $N_R = 20$ in the case of exponential correlation considering different correlation factors : $0.8, 0.95$ and 0.99.

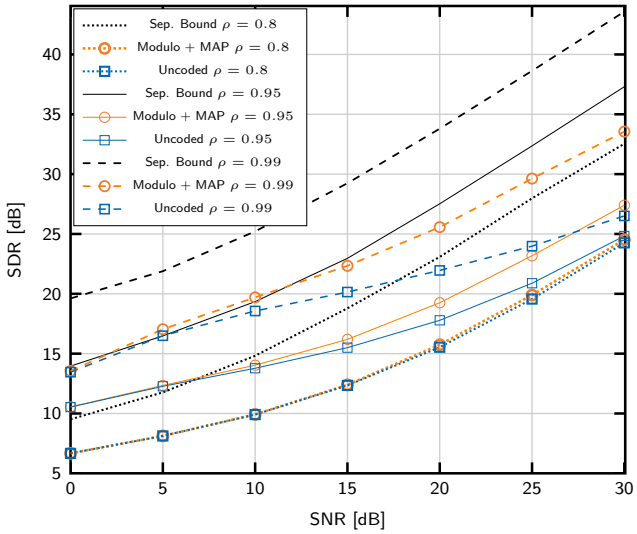

Fig. 10. SDR against SNR for $K = 10$ and $N_R = 20$ with equal correlation $\rho = 0.95$, and where the user powers are given by a log-distance path loss model.

parameters α_k can be used for the last decoded users, since for these users there is more prior information available about the transmitted symbols. Lower α_k parameters allow to increase the corresponding Δ_k values and, consequently, the overall MSE given by (24) will be smaller. It is interesting to remark that modulo mappings provide superior performance when the parameters are optimized with the channel strategy, since in this case the channel information is exploited to refine the optimization step. As observed in both figures, the gain due to the channel state optimization is about 1 dB. Finally, the performance curves corresponding to the mapping and the uncoded schemes, and the separation upper bound have similar slope when the number of receive antennas is larger than the number of MAC users. This reaffirms the assumption that modulo mappings are specially suitable for this type of scenarios. Finally, the gap between the system performance and the separation bound is larger than in the case of $N_R = 4$. Notice, however, that the distance between the real bound and the plotted one –considering only the sum-rate– is potentially larger as the number of users grows, since it is more likely that some individual constraint is violated.

In the next experiment, the performance of modulo mappings is evaluated considering an exponential correlation model, i.e., the correlation between the i-th and j-th source symbols is modeled as $\rho_{i,j} = \rho^{|i-j|}, \forall i, j$. We considered different correlation factors: $\rho = 0.8$, $\rho = 0.95$ and $\rho = 0.99$. In this case, the performance curves are obtained assuming a MAC scenario with $K = 10$, $N_R = 20$, MAP decoding and parameter optimization based on the channel state strategy. Fig. 9 compares the performance obtained with modulo mappings to that of the uncoded scheme and to the upper bound with source-channel separation. The performance for the uncoded transmission of uncorrelated sources, i.e. $\rho = 0$, is also included for comparison. As observed, the performance gain of modulo mappings with respect to the uncoded scheme is more remarkable when the correlation is higher, specially for medium and high SNRs. In fact, this gain is negligible for $\rho = 0.8$ in all the SNRs range, while it is about 6 dB for $\rho = 0.99$ and SNR $= 30$ dB. Moreover, all performance curves corresponding to uncoded transmission converge to the uncorrelated one as the SNR increases, regardless of the correlation level. These results suggest that the analog JSCC scheme with modulo encoding is able to exploit high correlations even for high SNR values, while the uncoded scheme does not improve the SDR in this regime. This is because the uncoded scheme uses linear MMSE decoding to estimate the source symbols and the weight of the correlation information in this strategy diminishes as the noise effect vanishes. Finally, the gap between the system performance and the separation bounds is constant for all SNRs, and it increases from 5 dB for $\rho = 0.8$ to almost 10 dB for $\rho = 0.99$.

We have until now assumed that all the MAC users transmit with the same power. We now move to a scenario with asymmetric power constraints and test the behaviour of the proposed analog JSCC system with modulo mappings in this situation. In particular, we choose a power allocation model that takes into account the propagation loss of radio signals over wireless channels. This model is useful to model, for example, a wireless sensor network where the nodes are placed at different distances from the central receiver. Specifically, we assume the k-th node is at a distance $d_k = k\ d$ where $d = d_1$ is the distance of user $k = 1$ which is the closest to the receiver. Assuming free-space propagation, this corresponds to a transmit power for the k-th node equal to $P_k = P d_k^{-2}$. SDR curves are plotted with respect to SNR $= P_1/\sigma_n^2$ which is the SNR for user $k = 1$.

We consider a MAC scenario with $K = 10$, $N_R = 20$, same correlation between the source symbols with $\rho = 0.8, \rho = 0.95$ and $\rho = 0.99$, MAP decoding and parameters optimization using the sphere decoder. Fig. 10 shows the SDR curves obtained for the modulo mappings and the uncoded scheme assuming $d_1 = 1$. The upper bounds corresponding to the source-channel separation are also included in the figure for reference. As observed, the proposed analog JSCC system pro-

vides again better performance than the uncoded scheme when the users transmit with different powers. Like in the previous experiments, the gain obtained with modulo mappings is larger as the correlation increases, and the uncoded scheme saturates for high SNRs and high correlation levels. Finally, the gap between the system performance and the separation bounds is similar to that when $K = 10$, $N_R = 20$ and equal transmit powers, and it ranges from 7 dB to 10 dB in the high SNR regime depending on the source correlation.

VI. Conclusions

In this work, we have addressed the use of modulo mappings for the transmission of multivariate Gaussian sources over fading MACs. We have investigated a MAP decoding strategy to estimate the user symbols. In addition, the use of a sphere decoder makes the implementation of the MAP estimation practical for a large number of users. Simulation results have shown that MAP decoding practically achieves the same performance as MMSE decoding, but with lower complexity, while it clearly outperforms ML decoding, specially for non-orthogonal access. Thereby, the proposed analog JSCC scheme, together with MAP estimation and sphere decoding, is a truly zero-delay low-complexity solution to reliably transmit correlated information over fading MACs, specially for scenarios with high correlation and where the number of receive antennas is larger than the number of users. An appropriate optimization of the mapping parameters also ensures that the analog JSCC system achieves equal or better performance than the uncoded scheme for all SNR regimes.

Appendix A
MMSE Estimator

As explained in Section III-2, the source pdf conditional to the vector of observed symbols can be expressed as

$$p(\tilde{\mathbf{s}}|\tilde{\mathbf{y}}) \propto p(\tilde{\mathbf{y}}|\tilde{\mathbf{s}})p(\tilde{\mathbf{s}}) = \sum_i q_i(\tilde{\mathbf{y}}, \tilde{\mathbf{s}})p(\tilde{\mathbf{s}}). \tag{41}$$

Using the definition of $q_i(\tilde{\mathbf{y}}, \tilde{\mathbf{s}})$ given by (16), and the piecewise definition of the modulo function in (9), the above expression is rewritten as

$$\begin{aligned} p(\tilde{\mathbf{s}}|\tilde{\mathbf{y}}) &\propto \sum_i \exp\left(-\frac{1}{\sigma_n^2}\|\tilde{\mathbf{y}} - \tilde{\mathbf{H}}\,\mathrm{f}_i(\tilde{\mathbf{s}})\|^2\right)\exp\left(-\frac{1}{2}\tilde{\mathbf{s}}^T\mathbf{C}_{\tilde{\mathbf{s}}}^{-1}\tilde{\mathbf{s}}\right) \\ &\propto \sum_i \exp\left(-\frac{1}{\sigma_n^2}\|\tilde{\mathbf{y}} - \tilde{\mathbf{H}}\boldsymbol{\Delta}(\tilde{\mathbf{s}} - \mathbf{A}\mathbf{l}_i)\|^2\right)\exp\left(-\frac{1}{2}\tilde{\mathbf{s}}^T\mathbf{C}_{\tilde{\mathbf{s}}}^{-1}\tilde{\mathbf{s}}\right). \end{aligned} \tag{42}$$

Developing this equation and reordering the resulting terms, we obtain

$$\begin{aligned} p(\tilde{\mathbf{s}}|\tilde{\mathbf{y}}) \propto& \sum_i \delta_i \\ &\cdot \exp\left(-\frac{1}{2}\left(\tilde{\mathbf{s}}^T\boldsymbol{\Sigma}^{-1}\tilde{\mathbf{s}} - \frac{1}{\sigma_n^2}2\tilde{\mathbf{s}}^T\boldsymbol{\Delta}^T\tilde{\mathbf{H}}^T(\mathbf{y} + \tilde{\mathbf{H}}\boldsymbol{\Delta}\mathbf{A}\mathbf{l}_i)\right)\right) \\ \propto& \sum_i \delta_i \exp\left(-\frac{1}{2}\left(\tilde{\mathbf{s}}^T\boldsymbol{\Sigma}^{-1}\tilde{\mathbf{s}} - 2\tilde{\mathbf{s}}^T\boldsymbol{\Sigma}^{-1}\boldsymbol{\mu}_i\right)\right), \end{aligned} \tag{43}$$

where

$$\delta_i = \exp\left(-\frac{1}{2\sigma_n^2}\|\tilde{\mathbf{y}} + \tilde{\mathbf{H}}\boldsymbol{\Delta}\mathbf{A}\mathbf{l}_i\|^2\right) \tag{44}$$

$$\boldsymbol{\Sigma} = \left(\frac{1}{\sigma_n^2}\boldsymbol{\Delta}^T\tilde{\mathbf{H}}^T\tilde{\mathbf{H}}\boldsymbol{\Delta} + \mathbf{C}_{\tilde{\mathbf{s}}}^{-1}\right)^{-1} \tag{45}$$

$$\boldsymbol{\mu}_i = \frac{1}{\sigma_n^2}\boldsymbol{\Sigma}\boldsymbol{\Delta}^T\tilde{\mathbf{H}}^T(\tilde{\mathbf{y}} + \tilde{\mathbf{H}}\boldsymbol{\Delta}\mathbf{A}\mathbf{l}_i). \tag{46}$$

The exponent can be rewritten as a quadratic form by adding and subtracting $\boldsymbol{\mu}_i^T\boldsymbol{\Sigma}^{-1}\boldsymbol{\mu}_i$, i.e.,

$$p(\tilde{\mathbf{s}}|\tilde{\mathbf{y}}) \propto \sum_i \phi_i \exp\left(-\frac{1}{2}\left(\tilde{\mathbf{s}} - \boldsymbol{\mu}_i\right)^T\boldsymbol{\Sigma}^{-1}\left(\tilde{\mathbf{s}} - \boldsymbol{\mu}_i\right)\right) \tag{47}$$

with $\phi_i = \exp\left(-\frac{1}{2}\left(\sigma_n^{-2}\|\tilde{\mathbf{y}} + \tilde{\mathbf{H}}\boldsymbol{\Delta}\mathbf{A}\mathbf{l}_i\|^2 - \boldsymbol{\mu}_i^T\boldsymbol{\Sigma}^{-1}\boldsymbol{\mu}_i\right)\right)$.

Appendix B
Sphere Decoder

Starting from the original metric given by

$$h(\mathbf{l}) = \frac{1}{2}\left(\sigma_n^{-2}\|\tilde{\mathbf{y}} + \tilde{\mathbf{H}}\boldsymbol{\Delta}\mathbf{A}\mathbf{l}\|^2 - \boldsymbol{\mu}_\mathbf{l}^T\boldsymbol{\Sigma}^{-1}\boldsymbol{\mu}_\mathbf{l}\right), \tag{48}$$

with $\boldsymbol{\mu}_\mathbf{l}$ defined in (28), and denoting $\mathbf{z} = \tilde{\mathbf{y}} + \tilde{\mathbf{H}}\boldsymbol{\Delta}\mathbf{A}\mathbf{l}$, this metric can be rewritten as

$$\begin{aligned} h(\mathbf{l}) =& \frac{1}{2}\left(\sigma_n^{-2}\|\mathbf{z}\|^2 - \frac{1}{\sigma_n^4}\mathbf{z}_i^T\tilde{\mathbf{H}}\boldsymbol{\Delta}\boldsymbol{\Sigma}\boldsymbol{\Delta}^T\tilde{\mathbf{H}}^T\mathbf{z}\right) \\ =& \frac{1}{2}\mathbf{z}^T\left(\frac{1}{\sigma_n^2}\mathbf{I} - \frac{1}{\sigma_n^4}\tilde{\mathbf{H}}\boldsymbol{\Delta}\boldsymbol{\Sigma}\boldsymbol{\Delta}^T\tilde{\mathbf{H}}^T\right)\mathbf{z} \\ =& \frac{1}{2}\mathbf{z}^T\left(\mathbf{I} + \frac{1}{\sigma_n^2}\tilde{\mathbf{H}}\boldsymbol{\Delta}\mathbf{C}_{\tilde{\mathbf{s}}}\boldsymbol{\Delta}^T\tilde{\mathbf{H}}^T\right)^{-1}\mathbf{z}, \end{aligned} \tag{49}$$

where the matrix inversion lemma was applied in the last step. Replacing back the definition of $\mathbf{z}$ and denoting $\mathbf{B} = \left(\mathbf{I} + \frac{1}{\sigma_n^2}\tilde{\mathbf{H}}\boldsymbol{\Delta}\mathbf{C}_{\tilde{\mathbf{s}}}\boldsymbol{\Delta}^T\tilde{\mathbf{H}}^T\right)^{-1}$, (49) can be written as

$$\begin{aligned} h(\mathbf{l}) =& \frac{1}{2}\left(\tilde{\mathbf{y}} + \tilde{\mathbf{H}}\boldsymbol{\Delta}\mathbf{A}\mathbf{l}\right)^T\mathbf{B}\left(\tilde{\mathbf{y}} + \tilde{\mathbf{H}}\boldsymbol{\Delta}\mathbf{A}\mathbf{l}\right) \\ =& \frac{1}{2}\left(\tilde{\mathbf{y}}^T\mathbf{B}\tilde{\mathbf{y}} + \mathbf{l}^T\mathbf{A}^T\boldsymbol{\Delta}^T\tilde{\mathbf{H}}^T\mathbf{B}\tilde{\mathbf{H}}\boldsymbol{\Delta}\mathbf{A}\mathbf{l} + 2\mathbf{l}^T\mathbf{A}^T\boldsymbol{\Delta}^T\tilde{\mathbf{H}}^T\mathbf{B}\tilde{\mathbf{y}}\right) \end{aligned} \tag{50}$$

Introducing the matrix $\boldsymbol{\Lambda} = \frac{1}{2}\mathbf{A}^T\boldsymbol{\Delta}^T\tilde{\mathbf{H}}^T\mathbf{B}\tilde{\mathbf{H}}\boldsymbol{\Delta}\mathbf{A}$, the expression above is transformed into

$$h(\mathbf{l}) = \frac{1}{2}\left(\tilde{\mathbf{y}}^T\mathbf{B}\tilde{\mathbf{y}} + 2\mathbf{l}^T\boldsymbol{\Lambda}\mathbf{l} + 4\mathbf{l}^T\boldsymbol{\Lambda}\mathbf{A}^T\boldsymbol{\Delta}^T\tilde{\mathbf{H}}^T(\tilde{\mathbf{H}}\boldsymbol{\Delta}\mathbf{A}\mathbf{A}^T\boldsymbol{\Delta}^T\tilde{\mathbf{H}}^T)^{-1}\tilde{\mathbf{y}}\right). \tag{51}$$

Defining $\mathbf{l}_o = \mathbf{A}^T\boldsymbol{\Delta}^T\tilde{\mathbf{H}}^T(\tilde{\mathbf{H}}\boldsymbol{\Delta}, \mathbf{A}\mathbf{A}^T\boldsymbol{\Delta}^T\tilde{\mathbf{H}}^T)^{-1}\tilde{\mathbf{y}}$, we obtain

$$\begin{aligned} h(\mathbf{l}) =& \frac{1}{2}\left(\tilde{\mathbf{y}}^T\mathbf{B}\tilde{\mathbf{y}} + 2\mathbf{l}^T\boldsymbol{\Lambda}\mathbf{l} + 4\mathbf{l}^T\boldsymbol{\Lambda}\mathbf{l}_o\right) \\ =& \frac{1}{2}\left(2(\mathbf{l} + \mathbf{l}_o)^T\boldsymbol{\Lambda}(\mathbf{l} + \mathbf{l}_o) - 2\mathbf{l}_o^T\boldsymbol{\Lambda}\mathbf{l}_o + \tilde{\mathbf{y}}^T\mathbf{B}\tilde{\mathbf{y}}\right). \end{aligned} \tag{52}$$

Notice that $\mathbf{l}_o^T\boldsymbol{\Lambda}\mathbf{l}_o$ and $\tilde{\mathbf{y}}^T\mathbf{B}\tilde{\mathbf{y}}$ do not depend on $\mathbf{l}$ and, therefore, these terms can be disregarded when minimizing $h(\mathbf{l})$. Hence, the metric employed for the sphere decoder simplifies to

$$h(\mathbf{l}) = (\mathbf{l} + \mathbf{l}_o)^T\boldsymbol{\Lambda}(\mathbf{l} + \mathbf{l}_o). \tag{53}$$

APPENDIX C
UPPER BOUND BASED ON SOURCE-CHANNEL SEPARATION

Although the assumption of optimality for source-channel separation does not hold for the MAC with correlated sources, this criterion will be used to determine a reference bound for analog JSCC communications. The separation bound is calculated by equating the source rate distortion region and the capacity region of the fading MAC.

Given a set of distortion targets $\mathbf{d} = [D_1, D_2, ..., D_N]^T$, the rate distortion region $\mathcal{R}(\mathbf{d})$ is the set of rate distortion functions corresponding to the individual sources, i.e. $R_k^D(D_i), k = 1, ..., K$, and by the sum-rate distortion function $R_{\text{sum}}^D(\mathcal{D})$. For the case of distributed encoding of bivariate Gaussian sources under the MSE distortion, this region is given by [27], [28]

$$\mathcal{R}_1^D(D_1) = \left\{(R_1, R_2) : R_1 \geq \log\left(\frac{1}{D_1}\left(1 - \rho^2 + \rho^2 2^{-2R_2}\right)\right)\right\}$$
$$\mathcal{R}_2^D(D_2) = \left\{(R_1, R_2) : R_2 \geq \log\left(\frac{1}{D_2}\left(1 - \rho^2 + \rho^2 2^{-2R_1}\right)\right)\right\}$$
$$\mathcal{R}_{\text{sum}}^D(D_1, D_2) = \left\{(R_1, R_2) : R_1 + R_2 \geq \log\left(\frac{(1-\rho^2)\beta(D_1, D_2)}{2D_1 D_2}\right)\right\}$$

with $\beta(D_1, D_2) = 1 + \sqrt{1 + \frac{4\rho^2 D_2 D_2}{(1-\rho^2)^2}}$. For scenarios with more than two source symbols, [29] provides the following lower bound for the sum-rate

$$R_{\text{sum}}^D(\mathbf{d}) = \min_{\mathbf{D_s}: d_{ii} \leq [\mathbf{d}]_i} \log\left(\frac{|\mathbf{C_s}|}{|\mathbf{D_s}|}\right), \tag{54}$$

where $\mathbf{D_s} = (\mathbf{C}_s^{-1} + \mathbf{B})^{-1}$, for some diagonal matrix $\mathbf{B}$, and $\mathbf{C_s}$ is the source covariance matrix. However, closed-form expressions for the individual rate distortion functions are unknown for $N > 2$. In this case, an upper bound for the OPTA can be computed by equating only the sum-distortion function to the sum-capacity of the MAC. In general, this bound will be optimistic since the individual rate constraints are not necessarily satisfied.

On the other hand, the capacity region of the MIMO MAC channel is defined by [30]

$$\sum_{k \in \mathcal{K}} R_k^C(\mathbf{H}_k) \leq \log\left|\mathbf{I} + \frac{1}{\sigma_n^2}\sum_{k \in \mathcal{K}} \mathbf{H}_k \mathbf{Q}_k \mathbf{H}_k^H\right| \quad \mathcal{K} \subset \{1, \ldots, K\}, \tag{55}$$

where $\mathbf{Q}_k$ represents the covariance matrix for the k-th user channel inputs, and must satisfy $\text{tr}(\mathbf{Q}_k) \leq P_k \ \forall k = 1, \ldots, K$. The sum-capacity of a SIMO MAC with non-cooperative users is

$$R_{\text{sum}}^C(\mathbf{H}) = \log\left|\mathbf{I} + \frac{1}{\sigma_n^2}\mathbf{H}\mathbf{P}\mathbf{H}^H\right|, \tag{56}$$

where $\mathbf{P} = \text{diag}(P_1, \ldots, P_K)$ is a diagonal matrix with the power constraints for the MAC users.

In general, the OPTA bound can be defined in terms of intersections between the rate distortion and capacity regions. For the case of two users, we state the following minimization problem

$$D_{\text{sum}}(\mathbf{H}) = \min_{D_1, D_2 : \mathcal{C}(\mathbf{H}) \cap \mathcal{R}(D_1, D_2) \neq \emptyset} D_1 + D_2 \tag{57}$$

where $\mathcal{C}(\mathbf{H})$ represents the capacity region while $\mathcal{R}(D_1, D_2) = \mathcal{R}_1^D(D_1) \cap \mathcal{R}_2^D(D_2) \cap \mathcal{R}_{\text{sum}}^D(D_1, D_2)$ is the corresponding rate distortion region for the bivariate Gaussian distribution. For $K > 2$, we will only consider the constraints on the sum rates for all users, due to the computational complexity of searching for the best intersection between regions in such case. Hence, the separation bound is calculated by equating (54) and (56), i.e.,

$$D_{\text{sum}}(\mathbf{H}) = \min_{\mathbf{d}: R_{\text{sum}}^D(\mathbf{d}) = R_{\text{sum}}^C(\mathbf{H})} \mathbf{1}^T \mathbf{d}, \tag{58}$$

and then averaging the obtained distortions for each channel realization to determine the optimum SDR, i.e. $\text{SDR}_{\text{opt}} = \mathbb{E}_{\mathbf{H}}[1/D_{\text{sum}}(\mathbf{H})]$.

REFERENCES

[1] C. E. Shannon, "A mathematical theory of communication," *The Bell System Technical Journal*, vol. 7, pp. 379–423, 1948.

[2] A. Lapidoth and S.Tingueley, "Sending a bivariate Gaussian over a Gaussian MAC," *IEEE Trans. on Information Theory*, vol. 56, no. 6, pp. 2714–2752, 2010.

[3] C. Tian, J. Chen, S. Diggavi, and S. Shamai, "Optimality and approximate optimality of source-channel separation in networks," *IEEE Transactions on Information Theory*, vol. 60, no. 2, pp. 904–918, Feb 2014.

[4] W. Zhong, Y. Zhao, and J. Garcia-Frias, "Turbo-like codes for distributed joint source-channel coding of correlated senders in multiple access channels," in *Signals, Systems and Computers, 2004. Conference Record of the Thirty-Seventh Asilomar Conference on*, vol. 1, Nov 2003, pp. 840–844 Vol.1.

[5] X. Zhu, Y. Liu, and L. Zhang, "Distributed joint source-channel coding in wireless sensor networks," *Sensors*, vol. 9, no. 6, p. 4901, 2009. [Online]. Available: http://www.mdpi.com/1424-8220/9/6/4901

[6] A. Abrardo, G. Ferrari, M. Martalò, M. Franceschini, and R. Raheli, "Orthogonal multiple access with correlated sources: Achievable region and pragmatic schemes," *IEEE Trans. on Communications*, vol. 62, no. 7, pp. 2531–2543, July 2014.

[7] C. E. Shannon, "Communication in the presence of noise," *Proceedings of the IRE*, vol. 37, no. 1, pp. 20–21, 1949.

[8] V. Kotel'nikov, *The theory of optimum noise immunity*. New York: McGraw-Hill, 1959.

[9] S. Y. Chung, "On the construction of some capacity-approaching coding schemes," *Ph.D. Dissertation, Dept. EECS*, 2000.

[10] T. A. Ramstad, "Shannon mappings for robust communication," *Telektronikk*, vol. 98, no. 1, pp. 114–128, 2002.

[11] F. Hekland, P. Floor, and T. A. Ramstad, "Shannon-Kotel'nikov mappings in joint source-channel coding," *IEEE Trans. on Communications*, vol. 57, no. 1, pp. 94–105, Jan 2009.

[12] G. de Oliveira Brante, R. Souza, and J. Garcia-Frias, "Analog joint source-channel coding in rayleigh fading channels," in *Proc. of Internation Conference on Acoustic, Speech and Signal Processing (ICASSP)*, May 2011, pp. 3148–3151.

[13] O. Fresnedo, F. Vazquez-Araujo, L. Castedo, and J. Garcia-Frias, "Low-complexity near-optimal decoding for analog joint source channel coding using space-filling curves," *IEEE Communications Letters*, vol. 17, no. 4, pp. 745–748, Apr 2013.

[14] X. Cai and J. W. Modestino, "Bandwidth expansion shannon mapping for analog error-control coding," in *40th Annual Conference on Information Sciences and Systems*, March 2006.

[15] B. Lu and J. Garcia-Frias, "Non-linear bandwidth reduction schemes for transmission of multivariate Gaussian sources over noisy channels," in *Information Sciences and Systems (CISS), 46th Annual Conference on*, March 2012.

[16] P. A. Floor, A. N. Kim, N.Wernersson, T. A. Ramstad, M. Skoglund, and I. Balasingham, "Zero-delay joint source-channel coding for a bivariate gaussian on a gaussian MAC," *IEEE Trans. on Comm.*, vol. 60, no. 10, pp. 3091–3102, Oct 2012.

[17] J. Kron, F. Alajaji, and M. Skoglund, "Low-delay joint source-channel mappings for the Gaussian MAC," *IEEE Communications Letters*, vol. 18, no. 2, pp. 249–252, Feb 2014.

[18] N. Wernersson, J. Karlsson, and M. Skoglund, "Distributed quantization over noisy channels," *IEEE Transactions on Communications*, vol. 57, no. 6, pp. 1693–1700, June 2009.

[19] E. Akyol, K. Rose, and T. Ramstad, "Optimized analog mappings for distributed source-channel coding," in *Proc. of IEEE Data Compression Conference*, 2010.

[20] M. S. Mehmetoglu, E. Akyol, and K. Rose, "Deterministic annealing-based optimization for zero-delay source-channel coding in networks," *IEEE Transactions on Communications*, vol. 63, no. 12, pp. 5089–5100, Dec 2015.

[21] P. A. Floor, A. N. Kim, T. A. Ramstad, and I. Balasingham, "Zero delay joint source channel coding for multivariate gaussian sources over orthogonal gaussian channels," *Entropy*, vol. 15, no. 6, pp. 2129–2161, 2013.

[22] N. Wernersson and M. Skoglund, "Nonlinear coding and estimation for correlated data in wireless sensor networks," *IEEE Transactions on Communications*, vol. 57, no. 10, pp. 2932–2939, October 2009.

[23] J. Karlsson and M. Skoglund, "Lattice-based source-channel coding in wireless sensor networks," in *2011 IEEE International Conference on Communications (ICC)*, June 2011, pp. 1–5.

[24] O. Fresnedo, P. Suárez-Casal, L. Castedo, and J. García-Frías, "Analog Distributed Coding of Correlated Sources for Fading Multiple Access Channels," submitted to IEEE Workshop on Statistical Signal Processing (SSP), 2016, Jun 2016.

[25] A. Genz and F. Bretz, *Computation of Multivariate Normal and t Probabilities*, ser. Lecture Notes in Statistics. Springer Berlin Heidelberg, 2009.

[26] B. M. Hochwald and S. ten Brink, "Achieving near-capacity on a multiple-antenna channel," *IEEE Transactions on Communications*, vol. 51, no. 3, pp. 389–399, March 2003.

[27] Y. Oohama, "Gaussian multiterminal source coding," *IEEE Transactions on Information Theory*, vol. 43, no. 6, pp. 1912–1923, Nov 1997.

[28] A. Wagner, S. Tavildar, and P. Viswanath, "Rate region of the quadratic Gaussian two-encoder source-coding problem," *IEEE Transactions on Information Theory*, vol. 54, no. 5, pp. 1938–1961, May 2008.

[29] J. Wang, J. Chen, and X. Wu, "On the Sum Rate of Gaussian Multiterminal Source Coding: New Proofs and Results," *IEEE Transactions on Information Theory*, vol. 56, no. 8, pp. 3946–3960, Aug 2010.

[30] D. Tse and P. Viswanath, *Fundamentals of Wireless Communication*. Cambridge University Press, 2005.